Nanoscale

Cite this: *Nanoscale*, 2012, **4**, 2900

www.rsc.org/nanoscale

PAPER

Bioinspired steel surfaces with extreme wettability contrast†

Eun Kyu Her,[ab] Tae-Jun Ko,[ab] Kwang-Ryeol Lee,[a] Kyu Hwan Oh[b] and Myoung-Woon Moon*[a]

Received 7th December 2011, Accepted 28th February 2012
DOI: 10.1039/c2nr11934j

The exterior structures of natural organisms have continuously evolved by controlling wettability, such as the Namib Desert beetle, whose back has hydrophilic/hydrophobic contrast for water harvesting by mist condensation in dry desert environments, and some plant leaves that have hierarchical micro/nanostructures to collect or repel liquid water. In this work, we have provided a method for wettability contrast on alloy steels by both nano-flake or needle patterns and tuning of the surface energy. Steels were provided with hierarchical micro/nanostructures of Fe oxides by fluorination and by a subsequent catalytic reaction of fluorine ions on the steel surfaces in water. A hydrophobic material was deposited on the structured surfaces, rendering superhydrophobicity. Plasma oxidization induces the formation of superhydrophilic surfaces on selective regions surrounded by superhydrophobic surfaces. We show that wettability contrast surfaces align liquid water within patterned hydrophilic regions during the condensation process. Furthermore, this method could have a greater potential to align other liquids or living cells.

1. Introduction

Natural organisms have been observed to continuously develop or evolve exterior structures that are simple and well-designed for living in certain environments.[1–5] Some organisms use their surface structures for adjusting wettability, such as the Namib Desert beetle, whose back has hydrophilic/hydrophobic patterning for water harvesting by mist condensation in dry desert environments, and some plant leaves that have hierarchical micro/nanostructures to achieve superhydrophobic, water-repellent effects.[1–7] The well-known "lotus effect" is attributed to a hierarchical structure and surface coating with epicuticular wax crystalloids,[4,5] which have been mimicked for scientific and industrial applications.[5,8,9] Superhydrophobic surfaces were rendered on various materials decorated with patterned micro- or nanostructures, such as carbon nanotubes, ZnO nanowires, anodically oxidized aluminium, nanostructured polymers, and patterned steels.[10–15] All of these surfaces have been reported to form characteristic micro/nano-patterns or degrees of hierarchical roughness.

In the case of metal surfaces, unlike hydrophilic surfaces that are easily fabricated by forming an oxide, making superhydrophobic surfaces requires additional processes for enhancing the surface roughness on the nano- or microscales, such as a chemical etching or high-temperature annealing of metals,[16,17] direct sculpturing using laser irradiation,[18] or electroless galvanic deposition on iron alloys or metals.[19] These fabrication techniques have undoubtedly opened up a new research field into superhydrophobic engineering with important, potential applications, though current applications are complex, expensive, and toxic, thus limiting large-scale production and further applications in practice.[10–12,16–23] It is also difficult to apply those methods to the fabrication of precise and sophisticated patterns with desired regions for further applications.

By controlling or tuning the surface energy on nanostructured or hierarchically structured surfaces, wettability can be easily tuned between superhydrophilicity and superhydrophobicity. Furthermore, the wettability contrast can be achieved through hydrophobic/hydrophilic surface domains in such a way as to mimick the back of the Namib beetle.[20] It has been reported that sol–gel coatings[21,22] or TiO_2/SiO_2 nanoparticles[23,24] can be used to pattern superhydrophilic/superhydrophobic surfaces for demonstration in several different systems, such as microfluidic devices or water-harvesting surfaces.[1,6,20–24] However, most materials or systems have employed polymeric or semiconductor materials due to the facile control of the morphology and surface energy.

In this work, we have developed a non-toxic, fast and room-temperature fabrication method for preparing superhydrophobic surfaces on alloyed steels decorated with nano-flake or needle patterns and covered with a hydrophobic material. In addition to the use of the plasma-based chemical vapor method at room temperature, our method is based on a non-toxic process through water treatment and an additional hydrophobic coating *via* dry

[a]*Future Conversion Technology Research Division, Korea Institute of Science and Technology, Seoul, 130-650, Korea. E-mail: mwmoon@kist.re.kr*
[b]*Department of Materials Science and Engineering, Seoul National University, Seoul, 151-742, Korea*
† Electronic supplementary information (ESI) available. See DOI: 10.1039/c2nr11934j

processing in comparison to previous methods that used toxic chemicals. Steel surfaces were fluorinated to play a role as a catalyst in the formation of Fe oxide during the water immersion process. Nanoneedle or flake shapes grow due to a continuous reaction between the fluorinated surface and water molecules.[25–27] Furthermore, the nanopatterns form cluster-like patterns at the micrometre scale after long immersion times, thereby producing a nano/microscale hierarchical structure that is similar to that of the acacia (*Robinia pseudoacacia*) leaf, as shown in Fig. 1a and b. The hydrophobic steels were characterized by measuring the wetting properties, such as the static contact angle (CA) and contact angle hysteresis (CAH). We demonstrated wettability contrast by forming superhydrophilic regions surrounded by superhydrophobic regions *via* selective oxygen plasma exposure of the superhydrophobic surfaces. The steel surfaces with extreme wettability contrast were used to align water droplets on hydrophilic regions for better water harvesting.

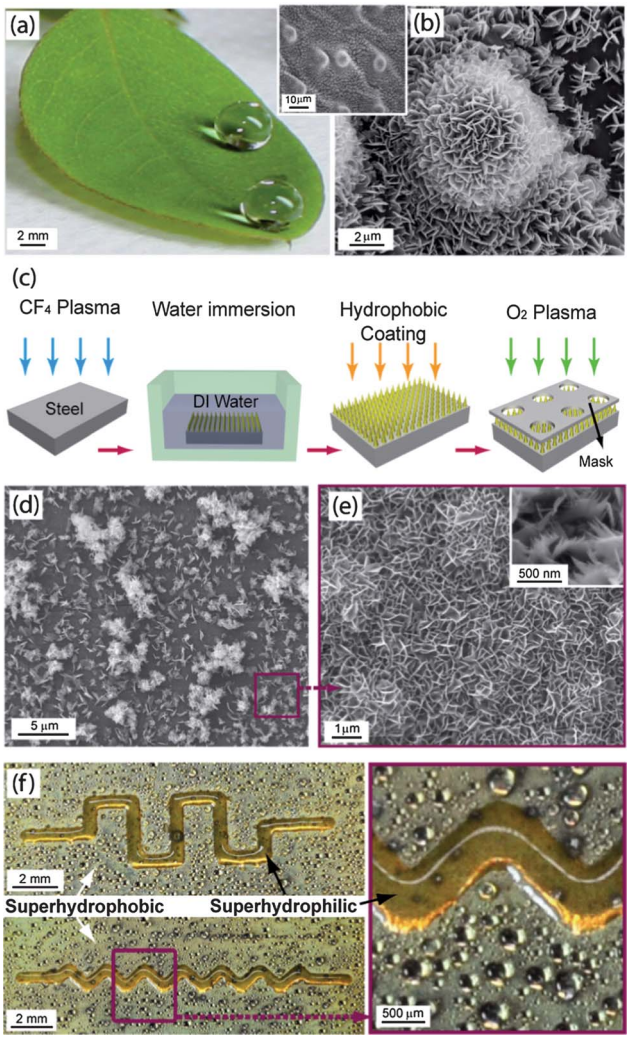

Fig. 1 (a) An optical micrograph of droplets on a *Robinia pseudoacacia* leaf surface and (b) SEM images of micro-nanostructures on the *Robinia pseudoacacia* leaf surface. (c) A schematic of fabrication procedure for superhydrophobic steel surfaces and mask patterning. SEM images of surface micro/nanostructures on a steel sample with lower (d) and higher (e) magnification for steel B (inset: magnified SEM image). (f) Optical micrographs of superhydrophobic/superhydrophilic-patterned steel, masked by a micro-channel after water condensation for 7 min and a magnified image around a microchannel from the boxed area.

2. Experimental

To fabricate superhydrophobic steel surfaces, a plasma-etching and coating method as well as a water immersion treatment were employed. Different steel alloys were purchased and are listed as steels A, B ($20 \times 20 \times 5$ mm^3, POSCO, Korea), and C (Fe foil, $20 \times 20 \times 0.1$ mm^3, Goodfellow, UK). The chemical compositions of steels A, B, and C are given in Table 1.

Samples were ultrasonically cleaned in ethanol after mechanical polishing. After drying with nitrogen, the samples were etched using a glow discharge of CF_4 gas with a treatment duration from 10 to 120 min by radio-frequency, plasma-enhanced chemical vapor deposition (r.-f. PECVD), as shown in Fig. 1c. The gas pressure and the bias voltage were maintained at 20 mTorr and -600 V_b, respectively. Then, the samples were immersed in deionized (DI) water and dried using a nitrogen gas blower prior to hydrophobic coating by PECVD. The duration of water immersion was varied between 10 and 120 min. To lower the surface energy of the nanostructured surfaces, a hydrophobic material (C:H:Si:O) was deposited on each surface using a precursor of hexamethyldisiloxane (HMDSO) by PECVD.[13–15] The gas pressure was fixed at 10 mTorr, the bias voltage was -400 V_b, and the coating time was 20 s.

We characterized the wettability of the modified steel surfaces by measuring the CA of DI water droplets. For these measurements, droplets of approximately 5 μL in volume (with radii of approximately 1 mm) were gently deposited on the substrate using a microsyringe. The advancing CA was measured by adding DI water to the sessile drop (~5 μL), and the receding CA was measured by the removal of water from a sessile DI water drop (~5 μL) using a microsyringe. The CAH was calculated as the difference between the measured advancing and receding CAs. All of the measurements were taken using a contact angle goniometer (Rame-Hart) in ambient air at 15 °C with a relative humidity of 20–35%. The reported CAs were collected by averaging the measurements from five different spots on each sample.

The micro- and nanostructures on the steel surfaces were observed with a scanning electron microscope (SEM, Hitachi, S-4100, Japan). The nanostructures and phase analysis of the surfaces were examined by a high-resolution transmission electron microscope (HR-TEM, Tecnai F-20, FEI). TEM samples were prepared in two ways. Firstly, cross-sectioning of the nanostructures was performed using a FE-SEM/FIB system (NOVA 200; FEI, Hillsboro, OR). Secondly, to collect a large amount of nanostructures, the sample surfaces were scratched, and the collected oxides were suspended in ethanol and dispersed

Table 1 Chemical compositions (wt%) of steel samples used in this work

	Fe	C	Si	Mn	Ni	Mo	Cr
Steel A	97.71	0.16	0.22	0.66	0.03	0.20	1.00
Steel B	88.49	0.50	1.45	0.54	—	—	9.00
Steel C	99.50	—	—	—	—	—	—

on a 300-mesh copper grid with a thin carbon film. For patterning of the superhydrophilic region on the superhydrophobic surface, stainless steel masks ($20 \times 20 \times 0.5$ mm^3) with different patterns were attached to the target surface of steel A. Oxygen-plasma treatment was performed on the mask-covered steel with a superhydrophobic surface (see Fig. 1c). A water condensation experiment was performed in a custom-made, humidity-controlled chamber. Water mist was supplied to the patterned steel for durations of 3 to 15 min, and images were obtained using a digital camera (Nikon, D300S, Japan).

3. Results and discussion

An acacia leaf was taken from a tree growing near our laboratory and was observed with an environmental scanning electron microscope (ESEM, FEI XL-30 FEG). Fig. 1a shows the droplet image on the superhydrophobic leaf surfaces with a CA of near 160° and a CAH of less than 10°. Koch *et al.* reported that the leaf surface has a hierarchical structure, *i.e.*, the surface structures consist of nanostructures on microstructures.[4,5,28] The hydrophobicity on this leaf surface is enhanced by wax components on the surface.

Wax platelets on *Robinia pseudoacacia* leaves are shown in Fig. 1b, which also shows that the leaf surface is covered with microscale bumps. The entire area, including the bumps and bases, is decorated with nanoflakes that are densely covered and arranged perpendicular to the surface. The nanoflake pattern reduces the contact area of water droplets or dust originating from the air. Similar patterns could be created on the surfaces of A and B steel (see the detailed chemical composition in Table 1). Based on plasma dry etching and water treatment, precise patterning of surface texturing was demonstrated on the steel surfaces, as shown in Fig. 1c (see the detailed experimental conditions in the ESI†).

Fig. 1d shows an SEM image of the as-modified steel B and its surface, which is covered with micro- and nanostructures. Nanoscale, needle-like structures are observed with diameters in the range of 20–40 nm and heights in the range of 1.5–3 μm, which were formed uniformly after CF_4 plasma–water immersion treatment (see Fig. S1†). It is also observed that microstructures of needle clusters were formed as the density of the nanoscale needle structures increased. In the case of steel B, a nanoflake structure predominantly evolved perpendicular to the steel surface with a height in the range of 0.7–1.0 μm, a width in the range of 400–800 nm, and a thickness in the range of 30–50 nm (Fig. 1e). In addition, dual-scale roughness on the micrometre-scale clusters (diameters of approximately 3 μm) composed of nanoscale flower and flake structures was observed.

Various shapes of superhydrophilic regions on superhydrophobic surfaces could be formed by varying the exposed-area configuration. Fig. 1f shows optical micrographs of water condensation results with two configurations of micro-channel patterns. Oxygen plasma-exposed regions are observed that are superhydrophilic and onto which water mist easily condensed within the hydrophilic region, while other regions remained superhydrophobic and exhibited droplets with spherical shapes. Further results are discussed in the last section of this work. Because of the simple and precise patterning process that results from applying selective plasma etching of a desired region on the steel surface, various and complex configurations of wettability patterning were produced.

SEM images in Fig. 2a–c reveal an effect of the water immersion duration and chemical composition on the formation of morphologies on steel. Initially, all three samples had smooth surfaces. It is also noted that flat surfaces with a hydrophobic coating only had a CA of ~95° and CAH of 40° for steels A and B and over 90° for steel C, similar to the reported value for an a-C:H:Si:O film having a lower surface energy of 24.2 mN m^{-1}, which is lower than that of the epicuticular wax covering lotus surfaces (30–32 mN m^{-1}).[13–15] With a fixed CF_4 plasma treatment of -600 V_b for 1 h, the water immersion duration was varied to induce morphological changes on the steel surfaces shown in Fig. 2a–c. For the 10 min water immersion treatment (top row), a porous and petaline-like shape was formed on the steel surfaces. On steels A and B, surface nanostructures were formed over the large area for an immersion duration of 30 min. After 60 min, steels A and B developed unique needle and flake structures, respectively, indicating that the pattern configuration is dependent on the alloy composition, as shown in the bottom row. However, the porous surface changed to a small sphere structure with a random distribution during water immersions between 10

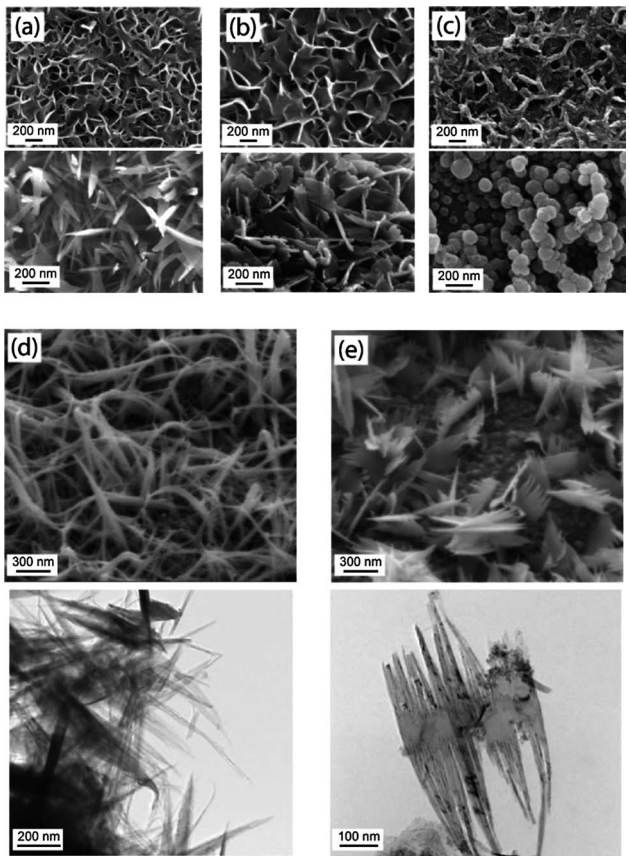

Fig. 2 SEM images of surface morphologies in different stages through water immersion on steel samples. (a) Steel A, (b) steel B, and (c) steel C. Each column indicates a different steel sample and each row indicates a different water treatment duration (top row for 10 min, bottom for 60 min). (d) Tilted SEM image and TEM image of nano-needles on steel A (e) Tilted SEM image and TEM image of nano-flakes on steel B. All samples were exposed to the same CF_4 plasma duration of 60 min.

and 60 min on steel C. It was found that nano-needles can be formed on steel A (Fig. 2d), while the nano-flake-type pattern appears with clusters of nano-needles on steel B, as confirmed by TEM observations (lower image in Fig. 2e), due to the different nature of the steel surfaces. Note that the upright flakes formed on steel B bear a close similarity in configuration to those on the plant in Fig. 1b.

Because metal oxides are hydrophilic, surface roughening with nanopatterns enhances hydrophilicity with a CA of less than 10°.[13–15] However, a surface coating with a low surface-energy material on flat or textured surfaces can alter the surface character from hydrophilic to hydrophobic or superhydrophobic.[13–15] When a water droplet is sitting on a near-top solid surface with a wetting-area roughness fraction of ϕ (= a partial wetting area divided by a projected area), the equilibrium condition for the water droplet can be considered to be in a Cassie–Baxter state, in which an apparent contacting line of the droplet obeys the following equation:[6,29,30]

$$\cos\theta_{app}^{c} = \phi\left(r_f \cos\theta_c + 1\right) - 1 \quad (1)$$

where r_f is the roughness ratio of the wet area and θ_c and θ_{app}^{c} are an equilibrium and apparent CA, respectively. The equilibrium eqn (1) states that as the wetting-area fraction, ϕ, decreases, the hydrophobicity increases. In this work, the individual nanostructure is sharpened from a sphere to a needle or flake as the water immersion duration increases, resulting in a lowering of the wetting area fraction. The wetting states of a water droplet on nanostructured steels were estimated on three different steels with hydrophobic coatings, as shown in Fig. 3a–c. The CA was nearly 150° on steels A and B at lower immersion durations of 30 min regardless of the CF_4 treatment time. Furthermore, the CAH remained below 10° after 30 min of water immersion on both steels. As the water immersion duration increased, steels A and B developed morphologies with a higher aspect ratio due to the shape change from a sphere to a needle and flake, which provide lower wetting-area fractions. However, the CA on steel C gradually increased up to 145° for a water immersion time of 120 min and a CF_4 treatment time of 60 min. As shown in Fig. 2c, the spherical particles on steel C have higher values of wetting-area fraction than those on steels A and B. These results indicate that nanostructures on steel surfaces with high aspect ratios and sharp edges further enhance the hydrophobicity (see the water repellent behavior in Movie S1†).

Structural and compositional analysis was performed with HR-TEM and XPS to investigate the crystallographic structure and morphology of the nanopatterns formed on steel A in Fig. 4. An HR-TEM image (Fig. 4a) revealed that the needle-like pattern is single-crystalline Fe_3O_4. The lattice spacing is approximately 0.256 nm, which is identical to the distance between the {311} crystallographic planes of the cubic phase of Fe_3O_4 (Fig. 4b) [JCPDS file no. 19-0629]. This result agrees well with the XPS analysis in Fig. S1a and b†. A thin oxide layer with a Cr deficit was found on the steel surface, on which nano-needles were expected to be initiated and grow. From the depth profile of the Energy Dispersive Spectrometry (EDS), the Fe content decreased with a relative increase in oxygen, while no Cr was detected in the needle structure, as shown in Fig. 4c and d.

In PECVD, high-energy electrons collide with gas molecules and create new species, and therefore many physical and chemical reactions occur, such as ionization, electronic excitation, and molecular fragmentation. A molecular dissociation and radical formation of CF_4 in the plasma would occur, and thus, CF^{3+} ions, electrons, and fluorine radicals (F^+) are generated and react with the target surfaces. Dissociated F radicals may be adsorbed

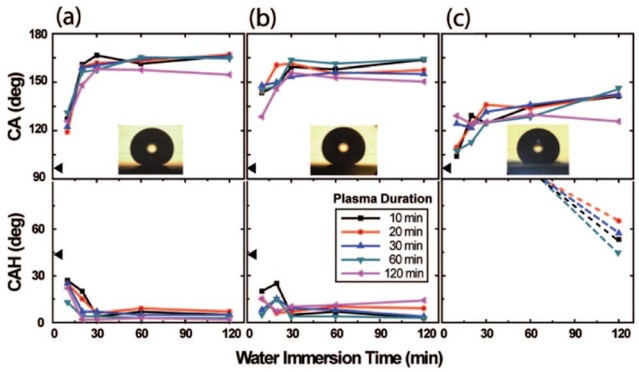

Fig. 3 Static CA and CAH were measured on the three different steel surfaces along with varying the duration of the CF_4 plasma treatment for the function of water immersion time. (a) Steel A, (b) steel B, and (c) steel C. Inset images were selected from samples that were treated with CF_4 plasma for 60 min and water immersion for 60 min. Note that CAHs on the steel C, not appearing in the graph, were measured as more than 90°. Black solid triangles in (a), (b) and (c) were taken on the steel surfaces with a hydrophobic coating only without plasma treatment and water immersion.

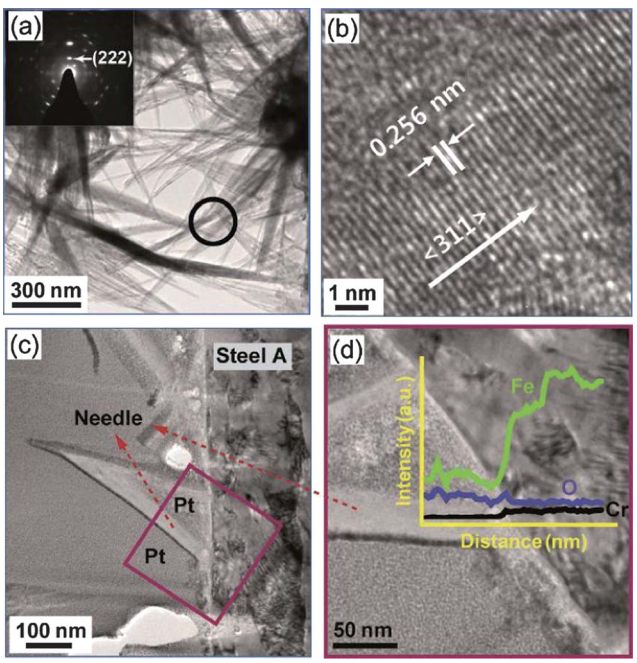

Fig. 4 HR-TEM and EDS analysis of nano-needle structures on steel A. (a) TEM images of nano-needle structures and electron diffraction pattern from the circled area. An inset of a HAADF image was taken from the black circle region. (b) An HR-TEM image of a single nano needle. (c) A TEM cross-sectional image of a steel surface with a nano-needle and (d) a magnified TEM cross-sectional image and depth profile of the chemical components obtained from the EDS line-scan.

on a target steel. Fluoride can react with Fe ions on the steel surface, forming Fe–F by chemical bonding. In the subsequent water immersion treatment, the fluoride can play a role as a catalyst for accelerating aqueous corrosion of Fe and Fe-based alloys.[25–27] Halide ions, in particular F, are known to play a catalytic role in accelerating aqueous corrosion of Fe-based steels in water.[25] Corrosion acceleration is attributed to the orders-of-magnitude faster rate of formation of the ligand complex between Fe–F and H_2O compared to that of a similar ligand complex between F-free Fe atoms and H_2O molecules in eqn (2), which follows:[27]

$$FeF + 5H_2O = [FeF(H_2O)_5]^+ + e^- \quad (2)$$

$$[FeF(H_2O)_5]^+ \quad (3)$$

$$[FeF(H_2O)_5]^+ + H_2O = [Fe(H_2O)_6]^{2+} + F^- \quad (4)$$

Due to instability in the species in eqn (3), the released F ion again drives the fast reaction to form another $[FeF(H_2O)_5]^+$ complex repeatedly, which leads to a classical catalytic role by F.[25–27] However, this process is inhibited by the Cr content on the steels, which results in a difference in the surface morphology of different alloy steels with respect to Cr content, as shown in Fig. 2a–c.

Selected regions were tuned to be superhydrophilic by oxygen plasma treatment on superhydrophobic surfaces, as shown in Fig. 5. Superhydrophobic surfaces were prepared with 60 min CF_4 treatments and water immersion durations of 60 min and subsequent hydrophobic coatings for 20 s. Upon oxygen plasma treatment for 10 s on the surface, the CA drastically decreased to less than 5 from 160°, thus becoming superhydrophilic. It is known that the hydrophilicity can be enhanced on nano-structured surfaces by the Wenzel state and hemi-wicking state.[29–32] It was also observed that the superhydrophilicity of oxygen plasma-treated surfaces was stable for 9–10 days with less than a 10° CA. Stainless steel masks with various holes for selective exposure to oxygen plasma (white area in pattern design) were used for superhydrophilic patterning, while unexposed regions (black area) remained superhydrophobic, which comprise the extreme wettability domains of the hydrophobic/hydrophilic patterns. This wettability control by contrasting hydrophobic/hydrophilic surfaces is similar to the wettability patterning inspired by the water-harvesting structure of the desert beetle's back, which has a hydrophilic region confined on a superhydrophobic surface.[2] Moreover, this surface may have more contrast in wettability due to the enhancement by the high aspect ratio nanostructures.

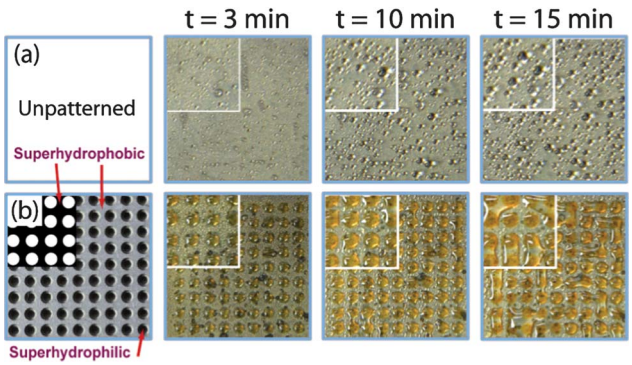

Fig. 5 Optical micrographs of condensation results under water mist on steel A. Condensed water droplets were observed on (a) unpatterned and (b) patterned steel surfaces for water condensation durations of 3, 10, and 15 min. Wettability contrast-patterned surfaces were created with different mask patterns with (b) an array of circle shapes (white regions) with diameters of 0.8 mm and spacings of 0.4 mm. Each image was taken with an area of 10 mm × 10 mm, and each inset was 4 mm × 4 mm.

Fig. 5 shows the water condensation process on unpatterned (Fig. 5a) and patterned (Fig. 5b, inner diameters of 0.8 mm) surfaces on steel A with an increase in water condensation duration under a high-humidity condition of RH 100%. In the case of unpatterned steel, water vapor condensed randomly, and the drop size was not selective regardless of the condensation duration. As the condensation duration increased from 3 to 15 min, the average diameter of droplets increased gradually from 0.11 to 0.24 mm on the unpatterned superhydrophobic surfaces. On wettability-patterned surfaces in Fig. 5b, the superhydrophilic regions rapidly condensed liquid droplets at the initial stage (less than 3 min) of the condensation experiment, while water droplets with high wetting angles coalesced and grew bigger on superhydrophobic regions with time. The nucleation rate on the hydrophilic surface would be significantly higher than that on the hydrophobic surface. It was reported that an estimate of the nucleation rate indicates that the nucleation rate on the hydrophilic surface with $\theta \approx 25°$ is a great many orders of magnitude ($\sim 10^{129}$) higher than that on the hydrophobic surface with $\theta \approx 110°$.[33] Condensed liquid water on the superhydrophilic regions increased in volume and was found to merge with liquid water on a neighboring superhydrophilic region, and liquid droplets formed on the superhydrophobic region, forming a water channel in Fig. 5b ($t = 15$ min).

Conclusions

In conclusion, superhydrophobic surfaces were fabricated on alloyed steels with different Cr contents using a method of plasma etching and subsequent water immersion treatment. High aspect ratio nanostructures, such as flakes or needles, were created with a catalytic reaction of fluorine ions by the water immersion process, forming Fe-oxide. A hydrophobic material with a-C:H:Si:O film was deposited on the micro- and nano-structured steel surfaces, and the material exhibited wetting angles of over 160° and hysteresis of as low as 10°. Wettability-controlled surfaces by contrasting hydrophobicity were introduced to harvest and align water droplets on confined regions with specific sizes. The wettability was patterned by selective-area oxygen plasma on micro- and nanostructured superhydrophobic surfaces.

Water droplets were well condensed to form liquids on the superhydrophilic regions with a good alignment in accordance with the repeated superhydrophilic/superhydrophobic array, and the size of the droplets was also confined by the area exposed to the plasma, guided by mask patterns with various shapes ranging from simple dot arrays to open microchannels.

It is expected that this facile, non-toxic, and fast technique to form a precise, wettability contrast pattern could be useful for large-scale production, as large as the size of a CVD cathode for

superhydrophobic engineering materials with industrial applications.

Acknowledgements

This study was financially supported by the MKE (10040003), Hyundai-Kia Motors Co. and KIST and in part by a grant from the Global Excellent Technology Innovation R&D Program funded by the MKE. OKH also acknowledges National Research Foundation of Korea (NRF) funded by the Ministry of Education, Science and Technology (R11-2005-065, OKH).

References

1 F. Xia and L. Jiang, *Adv. Mater.*, 2008, **20**, 2842–2858.
2 A. R. Parker and C. R. Lawrence, *Nature*, 2001, **414**, 33–34.
3 B. Bhushan and Y. C. Jung, *Prog. Mater. Sci.*, 2011, **56**, 1–108.
4 K. Koch and W. Barthlott, *Philos. Trans. R. Soc. London, Ser. A*, 2009, **367**, 1487–1509.
5 V. Zorba, E. Stratakis, M. Barberoglou, E. Spanakis, P. Tzanetakis, S. H. Anastasiadis and C. Fotakis, *Adv. Mater.*, 2008, **20**, 4049–4054.
6 A. Marmur, *Langmuir*, 2004, **20**, 3517–3519.
7 X. Zhang, F. Shi, J. Niu, Y. G. Jiang and Z. Q. Wang, *J. Mater. Chem.*, 2008, **18**, 621–633.
8 W. Barthlott and C. Neinhuis, *Planta*, 1997, **202**, 1–8.
9 Y. M. Zheng, D. Han, J. Zhai and L. Jiang, *Appl. Phys. Lett.*, 2008, **92**, 084106.
10 H. F. Meng, S. T. Wang, J. M. Xi, Z. Y. Tang and L. Jiang, *J. Phys. Chem. C*, 2008, **112**, 11454–11458.
11 J. M. Xi, L. Feng and L. Jiang, *Appl. Phys. Lett.*, 2008, **92**, 053102.
12 W. C. Wu, X. L. Wang, D. A. Wang, M. Chen, F. Zhou, W. M. Liu and Q. J. Xue, *Chem. Commun.*, 2009, 1043–1045.
13 T.-Y. Kim, B. Ingmar, K. Bewilogua, K. H. Oh and K.-R. Lee, *Chem. Phys. Lett.*, 2007, **436**, 199–203.
14 Y. Rahmawan, K.-J. Jang, M.-W. Moon, K.-R. Lee, K.-S. Kim and K.-Y. Suh, *Langmuir*, 2010, **26**, 484–491.
15 T. G. Cha, J. W. Yi, M.-W. Moon, K.-R. Lee and H.-Y. Kim, *Langmuir*, 2010, **26**, 8319–8326.
16 S. Wang, L. Feng and L. Jiang, *Adv. Mater.*, 2006, **18**, 767–770.
17 Z. Guo, F. Zhou, J. Hao and W. Liu, *J. Am. Chem. Soc.*, 2005, **127**, 15670–15671.
18 A. M. Kietzig, S. G. Hatzikiriakos and P. Englezos, *Langmuir*, 2009, **25**, 4821–4827.
19 I. A. Larmour, G. C. Saunders and S. E. J. Bell, *Angew. Chem., Int. Ed.*, 2007, **46**, 1710–1712.
20 L. Zhai, M. C. Berg, F. C. Cebeci, Y. Kim, J. M. Milwid, M. F. Rubner and R. E. Cohen, *Nano Lett.*, 2006, **6**, 1213–1217.
21 A. R. Abate, A. T. Krummel, D. Lee, M. Marquez, C. Holtze and D. A. Weitz, *Lab Chip*, 2008, **8**, 2157–2160.
22 A. R. Abate, J. Thiele, M. Weinhart and D. A. Weitz, *Lab Chip*, 2010, **10**, 1774–1776.
23 A. Kanta, R. Sedev and J. Ralston, *Langmuir*, 2005, **21**, 5790–5794.
24 X. Zhang, M. Jin, Z. Liu, D. A. Tryk, S. Nishimoto, T. Murakami and A. Fujishima, *J. Phys. Chem. C*, 2007, **111**, 14521–14529.
25 J. Gillardeau, Y. Macheteau, P. Plurien and J. Oudar, *Oxid. Met.*, 1970, **2**, 319–330.
26 H. M. Chung, W. E. Ruther, J. E. Sanecki, A. Hins, N. J. Zaluzec and T. F. Kassner, *J. Nucl. Mater.*, 1996, **239**, 61–79.
27 N. C. Huang and Z. J. Nagy, *J. Electrochem. Soc.*, 1987, **134**, 2215.
28 K. Koch, W. Barthlott, S. Koch, A. Hommes, K. Wandelt, W. Mamdouh, S. De-Feyter and P. Broekmann, *Planta*, 2006, **223**, 258–270.
29 A. B. D. Cassie and S. Baxter, *Trans. Faraday Soc.*, 1944, **40**, 546–551.
30 D. Quéré, *Annu. Rev. Mater. Res.*, 2008, **38**, 71–99.
31 R. N. Wenzel, *Ind. Eng. Chem.*, 1936, **28**, 988–994.
32 J. W. Yi, M.-W. Moon, S. F. Ahmed, H. Kim, T.-G. Cha, H.-Y. Kim, S.-S. Kim and K.-R. Lee, *Langmuir*, 2010, **26**, 17203–17209.
33 K. K. Varanasi, M. Hsu, N. Bhate, W. Yang and T. Deng, *Appl. Phys. Lett.*, 2009, **95**, 094101.